

The Volumetric Imaging System for the Ionosphere (VISION)

S. A. Budzien¹, K. F. Dymond¹, D. Chua¹, C. Coker¹, A. C. Nicholas¹, and S. E. Thonnard²

¹Space Science Division, Naval Research Laboratory, Washington, DC

²Office of Naval Research, Arlington, VA

THEME: Atmosphere-Ionosphere-Magnetosphere Interactions

SUMMARY

The Volumetric Imaging System for the Ionosphere (VISION) utilizes limb and nadir images to reconstruct the three-dimensional distribution of electrons over a 1000 km wide by 500 km high slab beneath the satellite with $10 \text{ km} \times 10 \text{ km} \times 10 \text{ km}$ voxels. The primary goal of the VISION is to map and monitor global and mesoscale ($> 10 \text{ km}$) electron density structures, such as the Appleton anomalies and field-aligned irregularity structures.

The VISION consists of three UV limb imagers, two UV nadir imagers, a dual frequency Global Positioning System (GPS) receiver, and a coherently emitting three frequency radio beacon. The limb imagers observe the O II 83.4 nm line (daytime electron density), O I 135.6 nm line (nighttime electron density and daytime O density), and the N₂ Lyman-Birge-Hopfield (LBH) bands near 143.0 nm (daytime N₂ density). The nadir imagers observe the O I 135.6 nm line (nighttime electron density and daytime O density) and the N₂ LBH bands near 143.0 nm (daytime N₂ density). The GPS receiver monitors the total electron content between the satellite carrying VISION and the GPS constellation and detects scintillation. The three frequency radio beacon will be used with ground-based receiver chains to perform computerized radio tomography below the satellite. Measurements made using the two radio frequency instruments may also be used for on-orbit calibration and validation of the VISION UV measurements.

1. INTRODUCTION

The Space Science Division at the Naval Research Laboratory has developed a program for characterizing the Earth's thermosphere and ionosphere based upon observing the naturally occurring airglow using ultraviolet sensors on space-based platforms. These sensors are passive in nature, so that there are no frequency management issues as is the case with topside sounders and radio beacons. In addition, with modern advances in multilayer filter design these sensors can be relatively compact.

We describe a new instrument concept developed at the NRL that will perform volumetric imaging of the Earth's ionosphere and thermosphere from a low-Earth orbiting satellite platform. This experiment is called the Volumetric Imaging System for the Ionosphere or VISION. The VISION is designed to map and monitor the three-dimensional distribution of mesoscale ($> 10 \text{ km}$) structures in the thermosphere and ionosphere. VISION will observe the Earth's limb and nadir and combine these measurements using tomographic techniques to infer the electron and neutral density over a 1000 km wide by 500 km thick slab of atmosphere beneath the satellite.

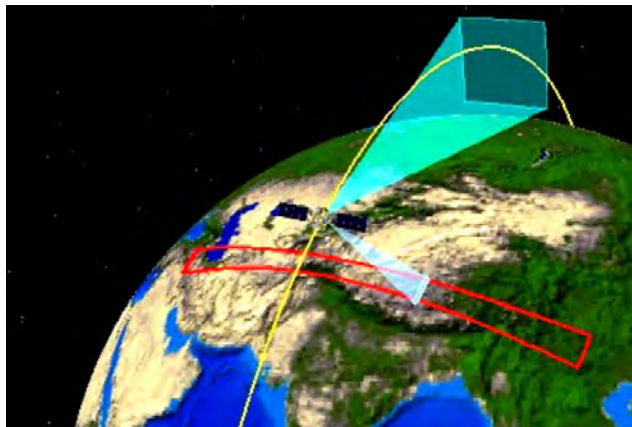


Figure 1: This shows the VISION concept of operation. The region that has been imaged by the cross-track scanner will be imaged by the limb imagers approximately 500 seconds later.

Report Documentation Page

Form Approved
OMB No. 0704-0188

Public reporting burden for the collection of information is estimated to average 1 hour per response, including the time for reviewing instructions, searching existing data sources, gathering and maintaining the data needed, and completing and reviewing the collection of information. Send comments regarding this burden estimate or any other aspect of this collection of information, including suggestions for reducing this burden, to Washington Headquarters Services, Directorate for Information Operations and Reports, 1215 Jefferson Davis Highway, Suite 1204, Arlington VA 22202-4302. Respondents should be aware that notwithstanding any other provision of law, no person shall be subject to a penalty for failing to comply with a collection of information if it does not display a currently valid OMB control number.

1. REPORT DATE 2011	2. REPORT TYPE	3. DATES COVERED 00-00-2011 to 00-00-2011			
4. TITLE AND SUBTITLE The Volumetric Imaging System for the Ionosphere (VISION)		5a. CONTRACT NUMBER			
		5b. GRANT NUMBER			
		5c. PROGRAM ELEMENT NUMBER			
6. AUTHOR(S)		5d. PROJECT NUMBER			
		5e. TASK NUMBER			
		5f. WORK UNIT NUMBER			
7. PERFORMING ORGANIZATION NAME(S) AND ADDRESS(ES) Naval Research Laboratory, Space Science Division, Washington, DC, 20375		8. PERFORMING ORGANIZATION REPORT NUMBER			
9. SPONSORING/MONITORING AGENCY NAME(S) AND ADDRESS(ES)		10. SPONSOR/MONITOR'S ACRONYM(S)			
		11. SPONSOR/MONITOR'S REPORT NUMBER(S)			
12. DISTRIBUTION/AVAILABILITY STATEMENT Approved for public release; distribution unlimited					
13. SUPPLEMENTARY NOTES					
14. ABSTRACT					
15. SUBJECT TERMS					
16. SECURITY CLASSIFICATION OF:			17. LIMITATION OF ABSTRACT	18. NUMBER OF PAGES	19a. NAME OF RESPONSIBLE PERSON
a. REPORT unclassified	b. ABSTRACT unclassified	c. THIS PAGE unclassified	Same as Report (SAR)	8	

It can also observe the northern and southern auroral ovals to better understand the energy deposition in these important atmospheric regions.

2. SCIENCE OVERVIEW

The VISION will attempt to answer several key science questions to help improve our understanding of the coupled ionosphere thermosphere system by providing both high spatial resolution (~10 km) and high sensitivity (~500 ct/s/Rayleigh). These characteristics in combination with its vantage point in low-Earth orbit (~1000 km altitude) make it an ideal platform for addressing the key science questions below.

Key Science Questions

What is the global response of the ionosphere and thermosphere to solar and geomagnetic forcing? The VISION will produce high spatial resolution limb and nadir imaging data that will be used to reconstruct the three dimensional electron distribution in the day and nighttime ionosphere. Knowledge of the volumetric electron density distribution can be used to study the complex coupling between the winds, electric fields, the Earth's magnetic field, and neutral and ion chemistry that determine the state of the ionosphere. The VISION data are gathered along the orbit track, as indicated in Figure 1.

How are ionospheric composition changes related to the underlying neutral thermosphere? The neutral atmosphere is the ultimate source of the ionosphere, so measurements of the volumetric distribution of the principal species in the thermosphere is also necessary to better understand the ionosphere. The F-region ionosphere is produced primarily by photoionization of O at altitudes below 150 km. This production is balanced by recombination loss. One of the principal recombination loss processes is charge exchange of the O⁺ with either N₂ or O₂ to produce N₂⁺ or O₂⁺, which rapidly recombine with ambient electrons. This charge exchange process is strongly dependent on the N₂ and O₂ densities, as well as the O⁺ density. The ratio of O to N₂ column densities has been observed to change during high geomagnetic activity. As this ratio decreases, the rate of photoionization of O decreases and the rate of recombination increases. Thus, the ionospheric electron density is expected to decrease because the production rate decreases and the loss rate increases. This has been observed using the *Dynamics Explorer* satellite (Strickland *et al.*, 2001). The DE data, however, do not have very high spatial resolution. The VISION will be able to perform studies like the DE studies but with simultaneous volumetric sampling of both the neutral and electron densities instead of the two-dimensional spatial mapping of DE. This will provide better understanding of how the changes in the O to N₂ species densities are reflected in the ionospheric electron density.

What are the characteristics, behavior, and origin of ionospheric bubbles and mid-latitude depletions? The mid- and low-latitude nighttime ionosphere sometimes develops strong mid- to small-scale ionospheric irregularities. These irregularities are caused by plasma

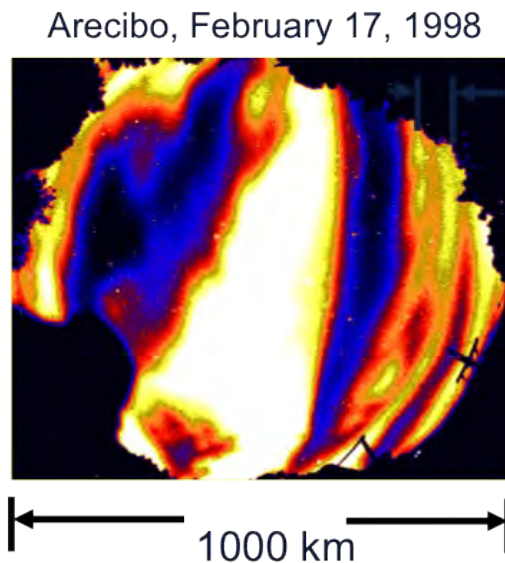


Figure 2: All sky camera image at 630 nm of a mid-latitude irregularity, acquired at the Arecibo Incoherent Scatter Radar Facility in Puerto Rico. The black irregular border is from near-field objects, such as trees and telephone poles. The bright bands running across the image from top to bottom are the undisturbed ionosphere. The dark bands running from top to bottom are ionospheric depletions or irregularities. These irregularities propagate in a southwesterly direction at 10-100 m/s. The electron density in these regions is nearly zero.

Data from 7/12/99 - Double Bubble (multiple vertical ionospheric depletions)
 GIMI Image: 12:47:12 UT, 30s
 LORAAS Data: 12:45:16 UT, 90s (15s missing)
 At 12:46:00, lat = -11°, lon = -162°, alt = 832 km

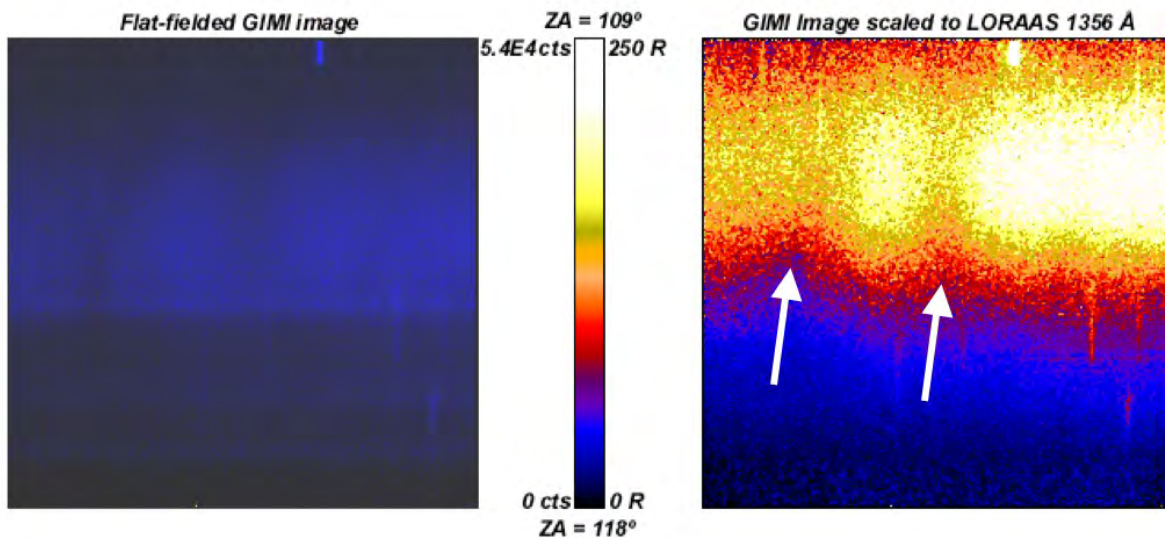


Figure 3: The left panel shows flat-field corrected data from the Global Imager of the Ionosphere (GIMI) experiment on the ARGOS satellite. The right hand panel shows the image after being converted to radiance units. The irregularities are indicated by the arrows in the image.

instabilities related to winds and electric fields. Figure 2 shows an all-sky camera map of a mid-latitude irregularity; this irregularity contains structures with 100 km dimensions. Figure 3 shows images of irregularities observed from space by the Global Imaging Monitor of the Ionosphere on the *Advanced Research and Global Observing Satellite (ARGOS)*. This image is of the Earth's limb and shows the vertical extent of two low-latitude irregularities. Using VISION, we hope to combine data sets like the two sets of images in Figure 2 and 3 to produce a three-dimensional reconstruction of the electron density. By knowing the local time of the bubble or irregularity, the scintillation properties can be predicted. VISION contains a tri-band (150, 400, and 1066.7 MHz) coherently radiating radio beacon with which to determine the electron density below the satellite using Computerized Ionospheric Tomography. In addition, the beacon can be used with the ground-based CIT receivers to study the scintillations caused by the irregularity.

How do the ionosphere and thermosphere respond to dynamical influences? Recent theoretical calculations have indicated that the troposphere and stratosphere can perturb the ionosphere and thermosphere. Ionospheric irregularity structures require a “seed” perturbation to initiate the instability. Winds, gravity waves, or electric fields may cause the necessary perturbations. Gravity waves may be induced by tropospheric dynamics. The effects of large tropospheric storms on the ionosphere and thermosphere cannot be observed from the ground, as the storm precludes gathering data. This is not a problem from space. This experiment will be able to look for ionospheric and thermospheric perturbations caused by tropospheric weather.

Daytime Observables

The principal ionospheric observable during the daytime will be the O II 83.4 nm lines. The O II 83.4 nm emission is produced principally by photoionization excitation of O at altitudes below 150 km. The 83.4 nm photons emitted downward are absorbed by the atmosphere. Those photons emitted upward enter the F-region ionosphere (altitudes 200–600 km) where they undergo multiple resonant scattering by

F-region O^+ ions. During the scattering process, the photons are entrapped and radiance field picks up a signature that is dependent on the altitude distribution of the O^+ ions. The VISION will primarily use the 83.4 nm emission to characterize the ionosphere at the Earth's limb.

The VISION will observe the O I 135.6 nm emission from neutral oxygen to infer the O density. On the dayside, this emission is primarily excited by photoelectron impact. However, there are contributions from radiative recombination and $O^+ - O^-$ mutual neutralization.

The VISION will measure the N_2 Lyman-Birge-Hopfield (LBH) band radiance near 143.0 nm to infer the N_2 density. This emission is excited solely by photoelectron impact. The 1403.0 nm bands are also near the peak of the O_2 Shumann-Runge continuum (Meier, 1991), which will allow the retrieval of the O_2 density by inversion of the limb measurements.

Nighttime Observables

The VISION will observe the O I 135.6 nm emission at night. This emission is excited primarily by radiative recombination of O^+ and electrons with a weaker contribution from $O^+ - O^-$ neutralization. The O^+ and therefore the electron density (by charge neutrality) can be inferred by inversions of the nighttime radiance. Tomographic inversion of the nighttime limb and nadir radiances will be used to produce the volumetric density field.

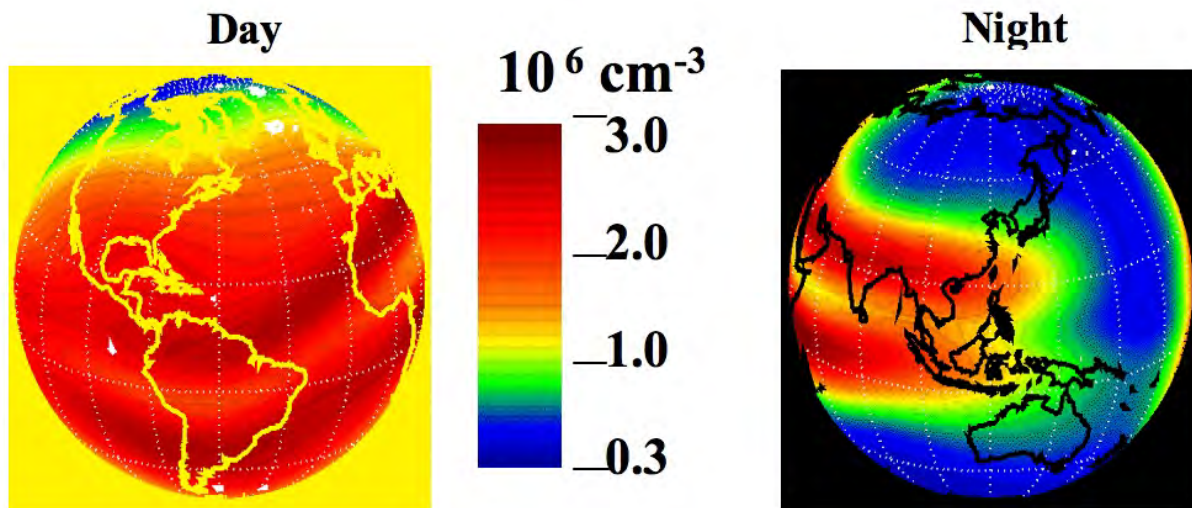


Figure 4: Map of the peak F-region electron density for mid-solar cycle conditions (10.7 cm flux of 140 solar flux units) at vernal equinox for day (left) and night (right). The peak density varies by an order of magnitude over the globe.

Radiances

Nighttime: The peak radiances were estimated by running the *International Reference Ionosphere* (IRI-90: Bilitza, 1990) for solar minimum and solar maximum conditions. Figure 4 shows a global map of the mid-solar cycle (10.7 cm solar flux of 140 solar flux units) peak electron density from the IRI-90. The radiances were then calculated by squaring the electron densities from IRI-90 and performing the line-of-sight integrations. The result was then scaled by the radiative recombination rate coefficients taken from Melendez-Alvira *et al.* [1999] and converted to units of Rayleighs. The limb radiances were derived from the nadir radiances by scaling them upward by a factor of 20 to account for limb brightening. The expected nadir radiances are: O II 83.4 nm less than 10 R, O I 135.6 nm between 0.1 R and 300 R (peak electron density $1 \times 10^5 - 5 \times 10^6 \text{ cm}^{-3}$), and N_2 LBH 143 nm approximately 0 R. The expected limb radiances are: O II 83.4 nm less than 10 R, O I 135.6 nm between 0.1 R and 3 kR, and N_2

LBH 143 nm approximately 0 R. Although the N₂ LBH and O II 83.4 nm emissions are excited by sunlight so the nighttime radiances are expected to be nearly zero, some O II 83.4 nm emission has been observed at night (*Chakrabarti et al.*, 1984). This emission is thought to be scattered over from the dayside by O⁺ ions in the magnetosphere.

Daytime: The nadir radiances were taken from *Meier* [1990]. The limb radiances were derived from these nadir radiances by scaling them upward by approximately a factor of 20 to account for limb brightening of the optically thin O I 135.6 and N₂ LBH 143.0 nm emissions. The O II 83.4 nm emission is optically thick and was instead scaled upward by approximately a factor of 2 to account for limb brightening. The expected limb radiances are: O II 83.4 nm between 1 R and 2 kR, O I 135.6 nm between 1 R and 20 kR, and N₂ LBH 143 nm between 1 R and 1 kR. The expected nadir radiances are: O II 83.4 nm between 1 R and 1 kR, O I 135.6 nm between 1 R and 1 kR, and N₂ LBH 143 nm between 1R and 100 R.

3. INSTRUMENT DESCRIPTION

The instrument design was driven by three basic requirements. First, the integration time to gather an image was selected to be 100 seconds or shorter for the limb imagers. The equatorial irregularities propagate Eastward at approximately 10–100 meters per second. The mid-latitude irregularities propagate southwesterly at 10–100 meters per second. The 100 second integration time ensures small smearing due to the irregularity's motion during an integration. Secondly, the limb imagers must image over 15° × 15° fields-of-view and the nadir imager must image along its 15° long slit at 0.5° spatial resolution. The 15° degree fields-of-view correspond to approximately 1000 km × 1000 km coverage at the limb. Thirdly, the experiment must have 10 km spatial resolution. The 10 km × 10 km resolution requires at least 100 resolution elements across the field-of-view. The spatial resolution requirement is driven by the requirement to spatially map irregularities that show spatial structures from the sub-kilometer level upward to the several thousands of kilometers. The electron densities vary from densities typical of the unperturbed ionosphere to nearly zero inside the depleted regions; this implies that the radiances vary from typical nighttime ionospheric radiances in the unperturbed regions to essentially zero in the depleted regions.

The VISION consists of three ultraviolet limb imagers operating at 83.4, 135.6, and 143.0 nm and a nadir cross-track scanner operating at 135.6 nm. During the daytime, the intensity gradients are much smaller than they are at night. Thus, the primary data sources during the daytime are the limb imagers. At night, the 83.4 nm and 143.0 nm signals are essentially zero, as the O II 83.4 nm and N₂ LBH emissions are excited by sunlight either directly by photoionization or indirectly by photoelectron impact. The primary nighttime data will be provided by the 135.6 nm cross-track scanner and the 135.6 nm limb imager.

Far-UltravioletLimb Imagers: The far-ultraviolet imagers consist of an off-axis parabolic telescope, which is fed by a three reflection filter assembly. The light is imaged onto an imaging microchannel plate detector. The detectors will be of the sealed tube type with a cesium-iodide photocathodes. The readout for the detector will be either a wedge-and-strip anode or a codacon. The telescope mirror is an 80 mm focal length, 2.5 cm diameter, first surface mirror with magnesium fluoride over aluminum coating on a zerodur blank. The filters are the three reflection bandpass filters developed for and flown on the Ultraviolet Imager (UVI) on the NASA POLAR satellite (*Zuckic et al.*, 1993). These filters have approximately 2.5 nm passbands (FWHM) and peak reflectances of 30–50%.

Extreme-Ultraviolet Limb Imager: The extreme-ultraviolet imager consists of a 80 mm focal length three mirror telescope with integral passband filters feeding an imaging microchannel plate detector. To further reduce the scattered light due to the bright Lyman-alpha geocorona, an indium/tin thin film filter will be used just prior to the detector face. The passband filters will be similar to those described in *Zuckic et al.* (1992).

Far-Ultraviolet Cross-Track Scanner: The far-ultraviolet cross-track scanner will consist of an off-axis parabolic telescope, which is fed by a three reflection filter assembly. The light is imaged onto an imaging microchannel plate detector. The detector will be of the sealed tube type with a cesium-iodide photocathode. The readout for the detector will be either a wedge-and-strip anode or a codacon. The telescope mirror is an 80 mm focal length, 50 mm diameter, first surface mirror with magnesium fluoride over aluminum coating on a zerodur blank. The filters are the three reflection bandpass filters developed for and flown on the Ultraviolet Imager (UVI) on the NASA *POLAR* satellite (Zuckic *et al.*, 1993). These filters have approximately 2.5 nm passbands (FWHM) and peak reflectances of 30–50%. The field-of-view will be scanned across the Earth's disk using a scanning mirror, which will be coated with magnesium fluoride over aluminum. The scan mirror must scan across 60° in 25 seconds. The scanner's slit subtends approximately 200 km when projected from the satellite at 1000 km altitude to 250 km. The satellite traverses this distance in approximately 26 seconds. The integration time of the cross-track scanner is then 0.2 seconds if the 10 km spatial resolution cross-track is to be maintained.

Sensitivity: We estimated the far-ultraviolet limb imager's sensitivity for the baseline design described above. The following formula was used to estimate the sensitivity of the FUV imager:

$$S = \frac{10^6}{4\pi} RTQA\Omega$$

where the reflectance of the mirror, R , is 0.8; the quantum efficiency of the detector, Q , is 0.1 (Siegmond *et al.*, 1987); the filter transmittance, T , is 0.5; the area of the primary mirror, A , is 5 cm²; the solid angle, Ω , is 0.063 steradians; and the constant $10^6/4\pi$ converts the results to Rayleighs. The resulting sensitivity at 135.6 nm is 1000 counts per second per Rayleigh. This sensitivity is approximately the same for the N₂ LBH 143 passband. During the daytime, this sensitivity will produce count rates that can damage the detector. The FUV limb imagers will be stopped down to reduce the entrance aperture area by an order of magnitude for the N₂ imager and by two orders of magnitude for the 135.6 nm imager.

We estimated the cross-track scanner's sensitivity for the baseline design described above. The following formula was used to estimate the sensitivity:

$$S = \frac{10^6}{4\pi} R^2TQA\Omega$$

where the reflectance of the mirror, R , is 0.8; the quantum efficiency of the detector, Q , is 0.1 (Siegmond *et al.*, 1987); the filter transmittance, T , is 0.5; the area of the primary mirror, A , is 20 cm²; the solid angle, Ω , is 2.3×10^{-3} steradians; and the constant $10^6/4\pi$ converts the results to Rayleighs. The resulting sensitivity at 135.6 nm is 117 counts per second per Rayleigh. During the daytime, this sensitivity will produce count rates that can damage the detector. The instrument will be stopped down to reduce the entrance aperture area by an order of magnitude.

The sensitivity of the EUV imager was estimated using the following formula:

$$S = \frac{10^6}{4\pi} RTQA\Omega$$

where the combined reflectance of the mirrors/filters, R , is 0.1 (reflectance from Zuckic *et al.*, 1992 scaled by a factor of 2); the quantum efficiency of the detector, Q , is 0.1 (Siegmond *et al.*, 1987); the indium/tin filter transmittance, T , is 0.1; the area of the primary mirror, A , is 5 cm²; the solid angle, Ω , is 0.063 steradians; and the constant $10^6/4\pi$ converts the results to Rayleighs. The resulting sensitivity at 83.4 nm is 25 counts per second per Rayleigh.

Signal-to-Noise Ratio: We estimated the signal-to-noise ratio for the sensitivities of the instruments from above combined with the minimum radiances from above. We assumed that there was negligible

dark count (reasonable for microchannel plate detectors with cesium iodide photocathodes) assuming 10×10 km pixels (dividing the total count rates by 10^4 pixels) and an integration time of 100 seconds. The following formula was used:

$$N = S\Delta t I / (10^4)$$

where S is the sensitivity; Δt is the integration time (100 s for the limb imagers and 0.2 s for the cross-track scanner); I is the minimum radiance; and 10^4 is the number of pixels in the image (30 for the long slit image of the cross-track scanner). The resulting numbers of counts for the limb imagers are: 0.25 counts at O II 83.4 nm, 10 counts at O I 135.6 nm, and 10 counts at N₂ LBH. Assuming the data are shot noise limited – the noise is the square-root of the number of counts, the signal-to-noise ratios for the limb imagers are: 0.5 at O II 83.4 nm, 3 at O I 135.6 nm, and 3 at N₂ LBH 143 nm. The resulting number of counts for the cross-track scanner is 0.07 counts for a signal-to-noise ratio of 0.26. Although the signal-to-noise ratio of the 83.4 nm limb imager and the cross-track scanner are less than the required signal-to-noise ratio of 3 set down as an observational requirement, they can be improved by accepting lower spatial resolution by binning pixels. This assessment is true only for the weakest signals, for the strongest signals there will be very high signal-to-noise.

4. SUMMARY

We presented an overview of Volumetric Imager of the Ionosphere (VISION) a new instrument being built by the NRL. This instrument is designed to infer the volumetric distribution of the ionospheric electron density and the thermospheric neutral density over a 1000 km wide by 500 km thick slab of atmosphere beneath the satellite. The VISION sensor characterizes the three-dimensional structure of the ionosphere to develop global climatology of irregularity occurrence, investigate the influence of the background ionosphere on irregularity formation, and study irregularity development and morphology. The VISION contains a dual-frequency GPS sensor and a tri-band coherently emitting radio beacon. These additional sensors provide validation of the VISION measurements. The tri-band frequency beacon can also be used to study the scintillations produced by the irregularities.

5. ACKNOWLEDGMENTS

We are indebted to G. R. Carruthers and P. Walker for providing the GIMI images and to J. J. Makela and M. C. Kelley of Cornell University for providing the ground based irregularity images. This work was supported by the Office of Naval Research through the Ionospheric Specification and Forecasting Accelerated Research Initiative.

6. REFERENCES

- Bilitza, D., *International Reference Ionosphere 1990*, National Space Science Data Center, NSSDC/WDC-A-R&S 90-20, Greenbelt, Maryland, 1990.
- Chakrabarti, S., Kimble, R., and Bowyer, S., "Spectroscopy of the EUV (350–1400 Å) Nightglow", *Journal of Geophysical Research*, **89**, 5660, 1984.
- Meier, R. R., "Ultraviolet Spectroscopy and Remote Sensing of the Upper Atmosphere", *Space Science Reviews*, **58**, No. 1 & 2, 1-186, 1991.
- Melendez-Alvira, D. J., Meier, R. R., Picone, J. M., Feldman, P. D., and McLaughlin, B. M., Analysis of the Oxygen Nightglow Measured by the Hopkins Ultraviolet Telescope: Implications for Ionospheric

- Partial Radiative Recombination Rate Coefficients, *Journal of Geophysical Research*, **104**, 14901, 1999.
- Siegmund, O. H. W., Everman, E., Vallerger, J. V., Sokolowski, J., and Lampton, M., "Ultraviolet Quantum Efficiency of Potassium Bromide as an Opaque Photocathode Applied to Microchannel Plates", *Appl. Optics*, **26**, No. 17, 1987.
- Strickland, D. J., Craven, J. D., and Daniell, R. E., "Global Enhancements in O/N₂ Recorded by the DE-1 FUV Imager During Geomagnetically Disturbed Periods", *Eos Trans. AGU*, **84** (20), Spring Meeting Suppl., Abstract SA62A-02, 2001.
- Zuckic, M., Torr, D., Kim, J., and Torr, M., "Extreme Ultraviolet Filters for 58.4 and 83.4 nm", Proc. SPIE **1744**, 178, 1992.
- Zuckic, M., Torr, D. G., Kim, J., Spann, J. F., and Torr, M. R., "Filters for the International Solar Terrestrial Physics Mission Far-Ultraviolet Imager", *Optical Engineering*, **32**, 3069, 1993.